

Vapor-phase cristobalite as a durable indicator of magmatic pore structure and halogen degassing: an example from White Island volcano (New Zealand)

C. Ian Schipper¹ · Céline Mandon¹ · Anton Maksimenko² · Jonathan M. Castro³ · Chris E. Conway⁴ · Peter Hauer⁵ · Martina Kirilova⁶ · Geoff Kilgour⁷

Received: 8 May 2017 / Accepted: 15 September 2017 / Published online: 3 October 2017
© Springer-Verlag GmbH Germany 2017

Abstract Vesicles in volcanic rocks are physical records of magmatic degassing; however, the interpretation of their textures is complicated by resorption, coalescence, and collapse. We discuss the textural significance of vesicle-hosted vapor-phase cristobalite (high-T, low-P SiO₂ polymorph), and its utility as a complement to textural assessments of magmatic degassing, using a representative dacite bomb erupted from White Island volcano (New Zealand) in 1999. Imaging in 2D (SEM) and 3D (CT) shows the bomb to have 56% bulk porosity, almost all of which is connected (~99%) and devoid of SiO₂ phases. The remaining (~1%) of porosity is in isolated, sub-spherical vesicles that have corroded walls and contain small (< 30 μm across) prismatic vapor-phase cristobalite crystals (98.4 ± 0.4 wt.% SiO₂ with diagnostic laser Raman spectra). Halogen degassing models show vapor-phase cristobalite to be indicative of closed-system chlorine and

fluorine partitioning into H₂O-rich fluid in isolated pores. At White Island, this occurred during shallow (< 100s of meters) ascent and extensive (~50%) groundmass crystallization associated with slow cooling in a volcanic plug. Pristine textures in this White Island bomb demonstrate the link between pore isolation and vapor-phase cristobalite deposition. We suggest that because these crystals have higher preservation potential than the bubbles in which they form, they can serve as durable, qualitative textural indicators of halogen degassing and pre-quench bubble morphologies in slowly cooled volcanic rocks (e.g., lava flows and domes), even where emplacement mechanisms have overprinted original bubble textures.

Keywords Cristobalite · Crystalline silica · Microtomography · Pyroclast textures · White Island

Editorial responsibility: J. Fierstein

Electronic supplementary material The online version of this article (<https://doi.org/10.1007/s00445-017-1157-1>) contains supplementary material, which is available to authorized users.

✉ C. Ian Schipper
ian.schipper@vuw.ac.nz

¹ School of Geography, Environment and Earth Sciences, Victoria University, PO Box 600, Wellington 6140, New Zealand

² Australian Synchrotron, 800 Blackburn Rd, Clayton, VIC 3168, Australia

³ Institute of Geosciences, University of Mainz, Becherweg 21, 55099 Mainz, Germany

⁴ Department of Geology and Paleontology, National Museum of Nature and Science, 4-1-1- Amakubo, Tsukuba, Ibaraki 305-0005, Japan

⁵ The MacDiarmid Institute for Advanced Materials and Nanotechnology, School of Chemical and Physical Sciences, Victoria University of Wellington, PO Box 600, Wellington 6140, New Zealand

⁶ Geology Department, University of Otago, PO Box 56, Dunedin 9016, New Zealand

⁷ Wairakei Research Centre, GNS Science, 114 Karetoto Rd, Taupo 3384, New Zealand

Introduction

Magmatic degassing exerts a fundamental control on volcanic eruptions, and is of central concern in many sub-disciplines of modern volcanology (Edmonds and Wallace 2017). The quantification of vesicle textures in two and three dimensions is a powerful way to investigate the physical manifestation of degassing as preserved in eruptive products (e.g., Shea et al. 2010; Baker et al. 2012). A holistic interpretation of vesicle textures must, however, take into consideration that different volatile species exsolve in varying proportions during a magmatic ascent (e.g., each is subject to different controls on solubility), and that bubble populations are susceptible to irreversible textural overprinting and modification (Thomas and Sparks 1992; Cashman and Mangan 1994; Stovall et al. 2010; McIntosh et al. 2014; Kennedy et al. 2016). To extract maximum data from the textures of eruptive products, it is desirable that multiple magmatic components (crystals, melt, bubbles) be used in parallel to investigate degassing signatures (e.g., Polacci et al. 2006; Sable et al. 2009; Murtagh and White 2013).

Cristobalite is a low-pressure, high-temperature polymorph of crystalline silica (SiO₂). Despite its nominal stability field being far outside the conditions that exist in crustal magma bodies (<0.2 MPa, 1470–1727 °C at 0.1 MPa; Heaney 1994), cristobalite forms and persists as a metastable secondary phase in many types of volcanic rocks. Volcanic cristobalite occurs as vapor-phase crystals and/or as a component in the devitrified groundmass of shallow intrusions, lava flows, and domes, and also within ash derived from silicic dome collapse (Swanson et al. 1989; Baxter et al. 1999; de Hoog et al. 2005; Horwell et al. 2010, 2013, 2014; Damby 2012; Schipper et al. 2015). Interest in volcanic cristobalite has been driven by (1) the possibility that it may occlude pores to compromise the stability of lava domes (Horwell et al. 2013; Boudon et al. 2015); (2) the fact that it is an example of metastable crystallization that challenges ideas of equilibrium phase stability from geochemical and crystallographic perspectives (e.g., Damby et al. 2014); and (3) concerns that volcanic cristobalite may be a respiratory hazard (e.g., Baxter et al. 1999; Horwell and Baxter 2006). Here, we examine another potentially useful characteristic of vapor-phase cristobalite: this being its theoretical ability to endure dynamic syn- and post-vesiculation flow processes that can modify and even obliterate the vesicles in which it forms (Schipper et al. 2015). In fact, we demonstrate strong links between pore connectivity (i.e., permeability), halogen degassing, and vapor-phase cristobalite formation that can aid in interpreting magmatic ascent and degassing histories.

We present textural and geochemical analyses of vapor-phase cristobalite in a pyroclastic dacite erupted in 1999 from White Island volcano (New Zealand). Although cristobalite is not abundant at White Island, its occurrence yields

information on the relationships between volcanic degassing, magmatic textural evolution, and metastable vapor-phase crystallization. These relationships potentially make vapor-phase cristobalite an easily identifiable and durable indicator of degassing processes, which can be upscaled from the bomb investigated here to lava flows and domes, as a good complement to textural analysis of vesicles and other crystals.

White Island

White Island (37.52° S, 177.18° E) is ~ 50 km north of the Bay of Plenty coastline, in the offshore extension of New Zealand's Taupo Volcanic Zone (Fig. 1a). It rises from approximately 350 m below sea level to 321 m above sea level, and is the summit of two overlapping andesitic-dacitic stratovolcanoes (Duncan 1970; Cole et al. 2000). There have been 41 reported eruptive periods at White Island since record keeping began in 1826 (Global Volcanism Program 2013), and at the time of writing, the volcano is in a state of minor unrest (GeoNet 2017). Most of the historical activity at White Island has been phreatic, phreatomagmatic, and Strombolian eruptions, with frequent reorganization of summit craters and fumaroles (Houghton and Nairn 1991). Although there have been many petrological and geochemical studies on White Island, none of these have documented cristobalite in eruption products (e.g., Duncan 1970; Cole et al. 2000; Severs et al. 2009).

The sample investigated here is from New Zealand's Geological and Nuclear Science (GNS Science) collection, and was ejected on April 20, 1999, as part of the eruption with Volcanic Explosivity Index (VEI) of 2 that started on August 21, 1998, from a vent in the NW corner of the crater complex (Global Volcanism Program 1998). The bomb (WIDP7) is texturally homogenous, and is the only existing material to have been collected from the April 1999 activity.

Analytical methods

Textures of the sample (WIDP7) were examined in 2D on a polished petrographic thin section using a flatbed scanner, petrographic microscope, and backscatter electron (BSE) imaging on a JEOL JXA-8230 Superprobe at Victoria University of Wellington. After thorough investigation at a range of magnifications, images collected at ×40 magnification in BSE were deemed sufficient for quantifying the full range of vesicles and microlites in the sample. Vesicles of interest (e.g., those that hosted vapor-phase cristobalite) were manually thresholded in Photoshop®, and their areas were measured in 2D using the Particle Analyzer plugin of ImageJ (Schneider et al. 2012). Microlite abundances were determined by 2D pixel counting in the same program.

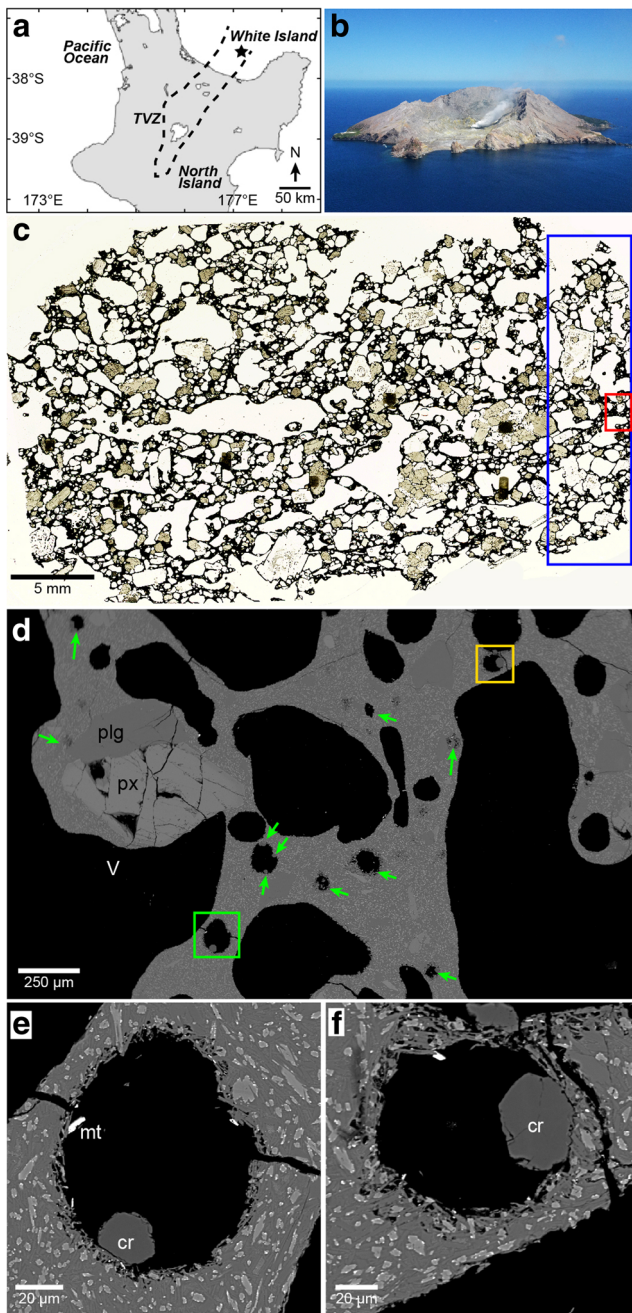


Fig. 1 Location and key textures in 2D. **a** White Island relative to the Taupo Volcanic Zone (TVZ) on the North Island of New Zealand. **b** White Island viewed from the southeast in December, 2016 (CI Schipper photo). Plume is rising from area of the main crater complex. **c** Flatbed scan of WIDP7 polished thin section. Red box indicates region of BSE image in **b**, blue box indicates portion of clast that was used for CT analysis (Fig. 2). **d** BSE image showing vesicles (V), pyroxene (px), and plagioclase (plg). Green and yellow boxes indicate regions shown in **e**, **f**, respectively. Cristobalite crystals indicated with arrows. Note that large amoeboid vesicles have relatively smooth walls and no cristobalite. **e**, **f** BSE images of cristobalite (cr) protruding from ragged, diktytaxitic walls of small, sub-rounded vesicles

A subsection of the billet from which the thin section was made was examined in 3D using synchrotron X-ray

source computed tomography (CT) at the Australian Synchrotron in Hutch 3B of the Imaging and Medical beamline using their “Ruby” detector with X-ray energy of 30 kV. Scans included the collection of 1800 radiographs with 0.8 s exposure time over 180° rotation. These were reconstructed with the in-house MASSIVE supercomputing cluster to yield rendered volumes with voxel edge length of 6 $\mu\text{m}/\text{pixel}$.

Vesicle and phenocryst abundances were determined from CT images by applying the voxel counter plugin of ImageJ. Connected and isolated pore spaces (vesicles) were segmented from each other using a fluid fill algorithm written by co-author Maksimenko (<https://github.com/antonmx/flood>). Isolated pores were segmented by applying a 3D version of the fluid-fill morphology algorithm, with a threshold selected to match void space, but not the solid material of the sample. The particle size used in the algorithm was set to two pixels to avoid leaking through thin walls. Inversion of the resulting mask and virtual subtraction of the material of the sample resulted in an image stack with the pores rendered to have a user-defined grayscale range, facilitating subsequent analysis and rendering. The volumes of isolated vesicles were determined in 3D using the threshold and label filter tools of Avizo 9.0 software, running on a local desktop computer in the Otago Centre for Electron Microscopy (OCEM). Additionally, the areas of isolated vesicles in each slice of the CT volume were measured in 2D using the Particle Analyzer plugin of Image J, for direct comparison with 2D data from BSE images. Rendering for visualization of textures in 3D was performed using the Drishti software package (Limaye 2012).

Major element concentrations in crystalline SiO_2 , bulk groundmass, and residual glass were determined by electron probe microanalysis (EPMA), with the JEOL JXA-8230 Superprobe. Silica crystals were analyzed (Si, Ti, Al, Na, K) using 15 kV, 12 nA, and a focused beam, standardized using synthetic pure oxides for each element. Groundmass (glass + microlites) was analyzed using 15 kV, 8.0 nA, and a spot size of 20 μm . Sodium was measured first, for shorter times and at a fixed peak position in order to minimize Na volatilization during analysis. The beam was defocused both to minimize Na loss and to encompass microlites and residual glass to yield a bulk (e.g., microlites + interstitial glass) groundmass composition. Analyses were standardized using natural and synthetic compounds, and verified in reference to basaltic glass standard VGA-99 (Jarosewich et al. 1980). Residual (interstitial) glass was analyzed for chlorine and fluorine as part of a subset of elements (SiO_2 , CaO, K_2O , Cl, F) using 15 kV, 25 nA, and a focused beam, standardized using synthetic CaF_2 (for fluorine) and a rhyolite

glass standard VG-568 (for chlorine; Jarosewich et al. 1980).

Groundmass H₂O contents were estimated using Fourier transform infrared spectroscopy (FTIR) with a Nicolet Continuum FTIR microscope at Massey University (New Zealand). Transmission infrared spectra in the range 4000–1200 cm⁻¹ were collected using a KBr beamsplitter, and a liquid nitrogen-cooled HgCdTe₂ (MCT) detector, on doubly polished wafers ranging in thickness from 80 to 100 μm, prepared following von Aulock et al. (2014). Background-corrected peak heights for total H₂O at 3530 cm⁻¹ were converted to concentrations using Beer's Law, with molar absorptivity of 75 mol⁻¹ cm⁻¹ (Okumura et al. 2003), density of 2.4 g cm⁻³ (calculated using groundmass composition and the method of Best 2003), and thicknesses as measured with a digital micrometer. The microlite content and resulting opacity of the wafers make them poorly suited to FTIR analysis, and these measurements should therefore be considered best estimates.

Mineral identification was performed in situ with laser Raman spectroscopy, using a Horiba JY LabRam HR800 at Victoria University, in the backscattering configuration, using a 633-nm He-Ne laser for excitation, a holographic notch filter, a 600-mm⁻¹ grating, and a liquid nitrogen-cooled charge-coupled device (CCD) detector. The laser power at the sample was 5 mW. Light was delivered and collected through an Olympus microscope objective with ×100 magnification (focal length 1.8 mm, numerical aperture 0.9), resulting in a probed area on the sample surface of approximately 1 μm diameter. The spectral resolution was approximately 3 cm⁻¹, and spectra were integrated over a 10-s acquisition time.

Results

The sample (WIDP7; Fig. 1c) is moderately vesicular, pyroxene-phyric, and plagioclase-phyric, with minor iron-titanium oxides. The majority of vesicles appear amoeboid (polylobate) in 2D, except for a subordinate population of small (< 100 μm diameter in cut section), sub-rounded vesicles. The groundmass is composed of 50 ± 10% interlocking plagioclase and clinopyroxene microlites with interstitial glass (Fig. 1d–f). The large amoeboid vesicles have walls that are mostly smooth (Fig. 1e), but occasionally show slight roughness from protruding microlites (Fig. 1f, bottom right). The sub-rounded vesicles are surrounded by 11 ± 2-μm diktytaxitic rinds, which have similar microlite abundances to the bulk groundmass (plag > cpx, total 47 ± 8%), but voids instead of interstitial glass. This

results in a localized zone of fine-scale porosity surrounding each of the sub-spherical vesicles (Fig. 1e, f).

Many of the sub-rounded vesicles have one or more prismatic crystals, 10–30 μm in length, protruding from their walls into their interiors (Fig. 1e, f). The crystals are colorless in plane-polarized light and isotropic in cross-polarized light, are darker than any other solid phase in BSE images, and fill < 15% of their host vesicle's volume (as estimated in 2D). Individual crystals usually appear pristine in thin section, lacking interior voids or inclusions, but occasionally have incipient fine-scale cracking with no preferred orientation. The amoeboid vesicles do not contain any such protruding crystals.

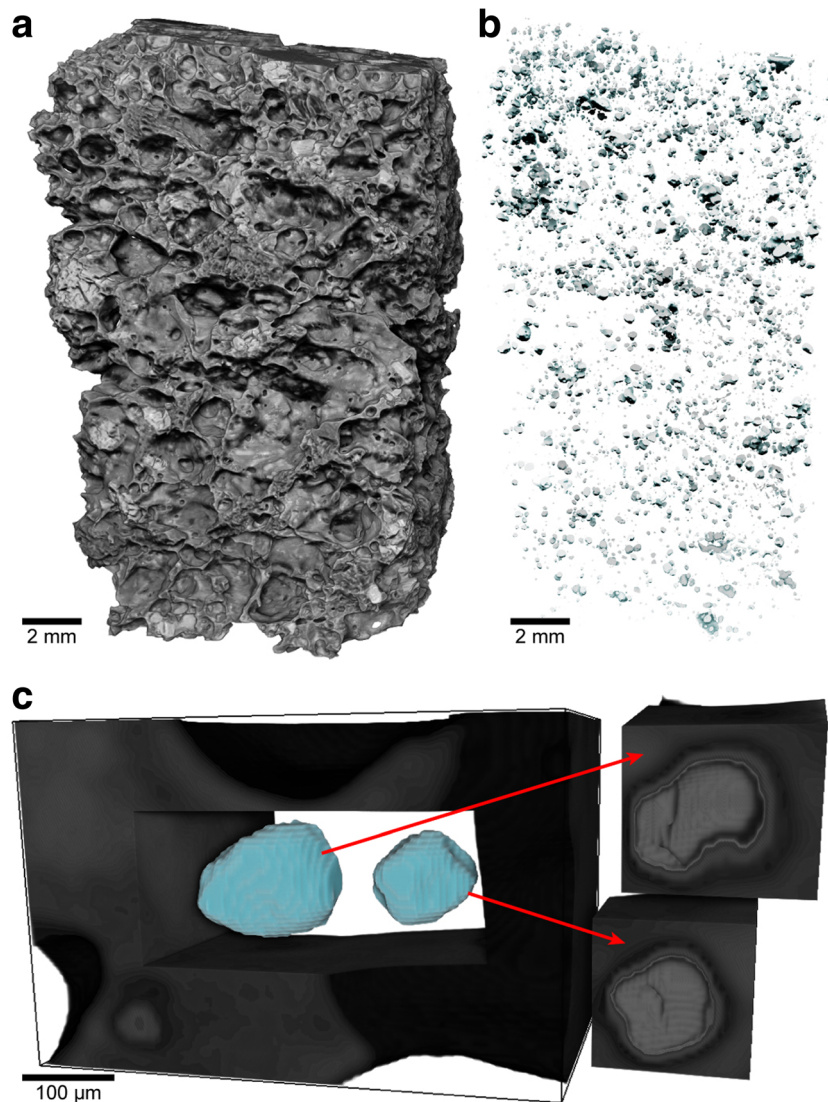
The total phenocryst content, as measured from CT scans, is 9% (clinopyroxene and plagioclase combined), or 20% when referenced to melt + crystals (e.g., excluding void space). Total porosity is 56%. Results from the fluid-fill algorithm indicate that 99% of this total porosity is connected into a single continuous void. The remaining 1% of the total porosity is in isolated vesicles (Fig. 2). Three-dimensional renderings showing only the isolated pores highlights that they have sub-spherical outer shapes (Fig. 2b, c) with spherical-equivalent diameters of 68 ± 52 μm (average ± 1 SD). Renderings of the interior of isolated vesicles show what appear to be sharp asperities protruding into the vesicle interiors (Fig. 2c), but further evaluation of these features is precluded by limitations on resolution and grayscale (density) segmentation.

To determine if the crystal-hosting, sub-rounded vesicles observed in BSE images (Fig. 1) correspond to the isolated, sub-spherical vesicles observed in CT scans (Fig. 2), we compare histograms of vesicle cross-sectional diameters as measured in 2D (Fig. 3). The use of 2D data allows direct comparison of the BSE and CT data without requiring stereological approximations to estimate vesicle volumes from 2D plane intersections (Shea et al. 2010). Both the crystal-hosting vesicles observed in BSE images and isolated vesicles in CT images have cross-sectional areas (expressed as the diameter of circle with an equivalent area) with bimodal distributions. Peaks are at 30–40 and 200 μm, and neither population contains vesicles larger than 500 μm.

EPMA analysis indicates that the protruding crystals within isolated vesicles are silica polymorphs, with SiO₂ of 98.4 ± 0.4 wt% (*n* = 67). The SiO₂ crystals have modest concentrations of other oxides, most notably 1.23 ± 0.23 wt% Al₂O₃ and 0.14 ± 0.04 wt% Na₂O (Table 1, Supplementary Table S1). Laser Raman analysis of the SiO₂ crystals shows strong peaks at 230 and 417 cm⁻¹, which are diagnostic of cristobalite (Kingma and Hemley 1994; Fig. 3a).

Bulk groundmass (e.g., microlites + interstitial glass) is dacitic (Le Maitre et al. 1989), with SiO₂ of

Fig. 2 CT volume renderings. **a** Portion of the clast with void space rendered transparent and solid opaque. **b** Rendered results of fluid-fill algorithm at same scale as **a**, with isolated pores shown in blue. **c** Closeup of solid volume (grayscale) with digital cutaway showing two isolated pores (blue). Right panels are inverted renderings of each of the isolated pores. Note that scale and segmentation limitations preclude isolation of individual cristobalite crystals, but that the isolated pores have asperities protruding from their inner walls



64.7 ± 0.94 wt% ($n = 25$; Fig. 5a; Table 1). Analysis of residual (interstitial) glass showed large ranges in all elements (e.g., 52.6–71.9 wt.% SiO_2 ; $n = 96$) because of the difficulty in placing the beam such that it completely avoided microlites. We have taken the ten most-evolved (highest SiO_2 and/or K_2O) residual glass analyses to be representative of the pure residual melt, where the focused beam was least contaminated by interaction with microlites (Fig. 5a; Table 1 and Supplementary Table S1). Melt inclusions in the studied bomb could not be analyzed because they were extensively decrepitated and crystallized.

The microcrystalline groundmass of the White Island bomb is poorly suited to analysis by FTIR, because its opacity causes poor infrared transmittance at high wavenumbers, and its heterogeneity makes the appropriate choices of molar absorptivity and density unclear. We therefore caution that our FTIR results should be taken only as indicative. The results do, however, show the bomb to be largely degassed with

respect to water, with a measured H_2O of 0.11 ± 0.04 ($n = 10$; Table 1) that is slightly lower than the 0.15 ± 0.1 wt.% matrix glass H_2O reported for White Island scoria from 1977 to 1989 (Wardell et al. 2001; Rapien et al. 2003).

Interpretations and discussion

Vapor-phase cristobalite in isolated pores

Based on their optical properties (Deer et al. 1992), laser Raman spectra (Fig. 4), and similarity to previously described examples (Damby 2012; Horwell et al. 2013), the SiO_2 crystals protruding from isolated vesicle walls in the White Island bomb are interpreted to be cristobalite deposited from a silica-saturated vapor (“vapor-phase cristobalite”). The White Island cristobalite crystals differ from previously reported examples

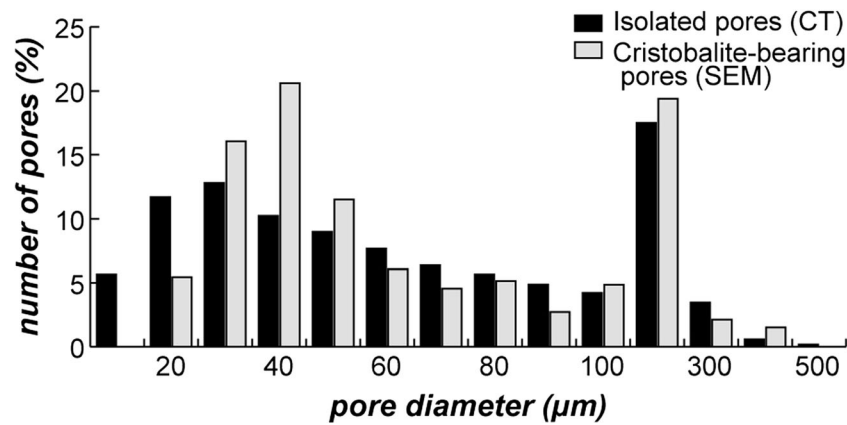


Fig. 3 Pore size distributions measured from CT and BSE images. The area of each segmented pore was measured, and is reported as the diameter of a circle of equivalent area. From CT data, only the isolated pores that were identified with the fluid-fill algorithm were measured, on each slice of the image stack (number of measured pores = 10^5). From BSE images, cristobalite-bearing pores were manually segmented on a

series of ten images ($n = 330$). Both types of pores have similar bimodal histograms, showing that the isolated pore population viewed in 3D is the same as the cristobalite-bearing pore population viewed in 2D. Extension of CT data to smaller sizes reflects the fact that the fluid-fill algorithm also identifies small voids at cracks in phenocrysts as isolated pores

in that they have non-developed or only poorly developed “fish scale” cracking that is considered to be a diagnostic feature (e.g., Horwell et al. 2013). The diktytaxitic rims surrounding each host vesicle in the White Island bomb are identical to those that have been previously interpreted as

corrosion rinds, from which interstitial glass has been physically consumed preferentially to more resistant microlites, providing the source of SiO_2 that was subsequently deposited as cristobalite (Damby 2012). Slight corrosion is apparent in some areas of the connected pore network (e.g., Fig. 1f, lower right); however, this is limited only to the protrusion of individual microlite tips. It is noteworthy that the persistence of the microlites allows identification of the corrosion rinds; corrosion in a microlite-free continuous melt would likely not be preserved texturally. The White Island bomb investigated here is a singular example, but has key features that clarify previously ambiguous aspects of volcanic cristobalite formation.

Table 1 Compositions

	Cristobalite	Groundmass	Residual glass ^a
EPMA			
SiO_2	98.3 (0.40)	64.7 (0.94)	71.5 (1.04)
TiO_2	0.12 (0.02)	0.36 (0.04)	–
Al_2O_3	1.23 (0.23)	15.0 (1.46)	–
FeO^f	–	3.27 (0.76)	–
MnO	–	0.35 (0.23)	–
MgO	–	1.98 (0.94)	–
CaO	–	5.41 (0.61)	1.74 (0.52)
Na_2O	0.14 (0.04)	3.01 (0.49)	–
K_2O	0.09 (0.06)	2.82 (0.22)	4.53 (0.30)
Cr_2O_3	–	0.01 (0.01)	–
Cl (ppm)	–	–	1533 (185)
F (ppm)	–	–	524 (170)
Total	99.9 (0.25)	97.0 (0.98)	–
<i>n</i>	67	25	10/96
FTIR			
H_2O	–	0.11 (0.04)	–
<i>n</i>	–	10	–

All values in weight percentage except where indicated. Values in brackets are 1 standard deviation. All EPMA data is given in Supplementary Table S1

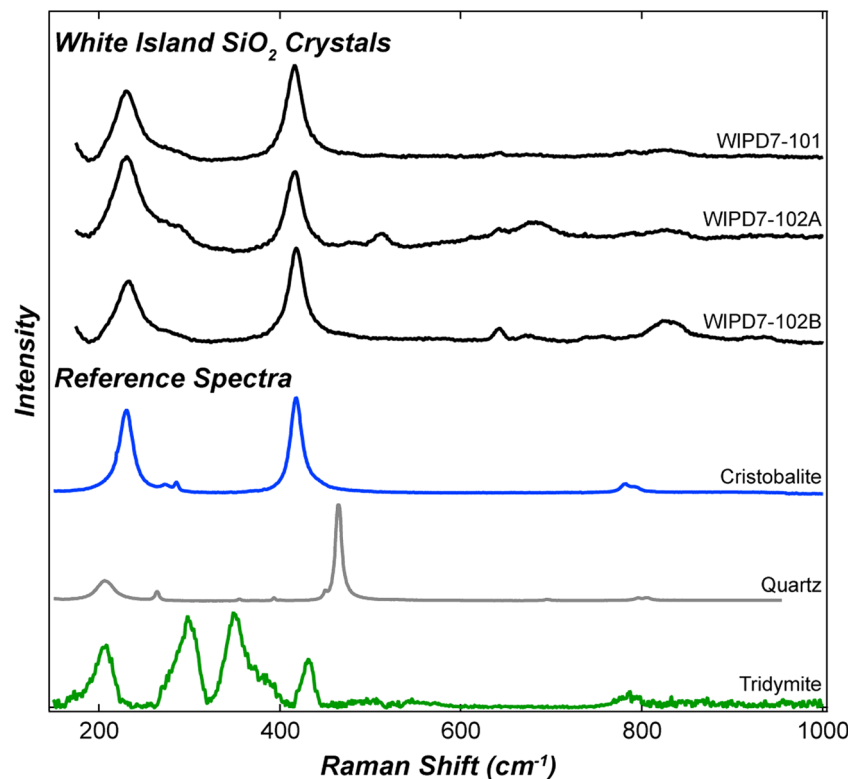
FeO^f total Fe, – not determined

^a Residual glass is the average of ten most evolved (highest SiO_2 and/or K_2O) spot analyses

Previous work on lava domes has shown volcanic cristobalite to occur both as vapor-phase crystals in pores and as a component of devitrified groundmass (e.g., Baxter et al. 1999). The coexistence of these has made it unclear whether they form independently or cooperatively (Horwell et al. 2013), although it has been noted that in particularly cristobalite-rich samples, the majority can be attributed to devitrification (Damby 2012). The White Island bomb contains only vapor-phase cristobalite, and does not show any devitrification. This provides evidence that vapor transport and deposition of SiO_2 and groundmass devitrification can occur independently (if perhaps concurrently in some settings).

Previous studies have discussed the length scales over which silica is redistributed as vapor-phase cristobalite in volcanic systems. In their study of volcanic domes, Horwell et al. (2013) introduced the concepts of “local redistribution,” where silica is leached from the groundmass around individual vugs and is then deposited from the vapor within the same pore, versus “bulk transport,” where silica is transported into a lava dome from below or outside the dome itself. Schipper et al. (2015) argued for the importance of local redistribution, identifying abundant vapor-phase cristobalite in isolated pores of a rhyolite lava flow

Fig. 4 Laser Raman spectra from three White Island SiO_2 crystals compared to reference spectra for SiO_2 polymorphs, cristobalite (Kingma and Hemley 1994), quartz (Gillet and Le Cléac'h 1990), and tridymite (Kingma and Hemley 1994)



that was rootless with respect to a sustained flux of deeper-derived gas. However, connected pores in some facies of the same lava flow also contained cristobalite, suggesting either that local redistribution does not occur exclusively or that extensive vesicle modification during lava emplacement (e.g., by shear coalescence, compaction) had obscured the relative timing of permeability development and cristobalite formation.

Qualitative observations and quantification of pore sizes in 2D show that the cristobalite-bearing pores observed in BSE images are the same pores that are seen to be isolated in 3D (Fig. 3). Therefore, cristobalite in the White Island bomb is exclusively in pores that are isolated from the main network. The isolated pores themselves are noteworthy for having spherical shapes (Figs. 1 and 2) that are typical of bubbles growing in a continuous melt where surface tension dominates over coalescence, shear, or other processes of modification (Rust et al. 2003). The open, connected pore network does not show any regions of high curvature that might suggest pinching or decoalescence had occurred, so it is most tenable that the isolated, cristobalite-bearing pores were never part of the larger, cristobalite-free, connected pore network. This White Island example therefore demonstrates the effectiveness of “local redistribution” of silica (sensu Horwell et al. 2013) for generating vapor-phase cristobalite, and the necessity of having an impermeable pore structure that promotes sustained contact between the corroding/depositing vapor and the bubble walls with which they react.

The rates at which vapor can corrode glass are poorly constrained, especially at magmatic temperatures. However, data compiled by Schipper et al. (2015; their Fig. 7) suggests that the $\sim 10\text{-}\mu\text{m}$ corrosion rims observed here could be achieved in as little as hours to days, depending mainly on the nature of the attacking species. The subsequent timescale over which SiO_2 is deposited from a Si-saturated vapor is also unknown. Timing is clearly an important control on cristobalite formation, and one that warrants experimentation. Horwell et al. (2014) noted that cristobalite abundance of dome-derived ash scaled with dome residence time, and Schipper et al. (2015) noted the most cristobalite-rich facies of the Cordón Caulle lava flow were the most slowly cooled. In the White Island example shown here, we note that the vapor-phase cristobalite crystals are relatively small ($< 30\ \mu\text{m}$) compared to those in extensive lava flows ($> 150\ \mu\text{m}$; Schipper unpublished data) and have poorly developed fish-scale cracking. We suggest that this represents a comparatively short growth history for the White Island cristobalite commensurate with cooling in a volcanic plug whose cooling history was truncated by the explosive fragmentation that produced the bomb, versus very slow cooling in large extrusive lava bodies. Similar dynamics, by which a cooling and crystallizing volcanic plug is subsequently disrupted by fresh, rapidly decompressing magma from below, have also been described for departures from normal background activity at Stromboli volcano, Italy (Gurioli et al. 2014).

Halogen degassing at White Island

The potential of chlorine and fluorine species to transport silica and deposit vapor-phase SiO_2 have been discussed (see review by Horwell et al. 2013). In the chlorine system, silica is transported mainly as SiCl_4 at $< 750^\circ\text{C}$ (Shmulovich et al. 2006), and in the fluorine system as SiF_4 at $< 900^\circ\text{C}$ (Churakov et al. 2000; de Hoog et al. 2005). Availability of one and/or other of these halogen species can therefore be considered a prerequisite to vapor-phase cristobalite formation. Because HCl is generally more abundant than HF in silicic systems, it has been suggested that degassing of chlorine is more important for silica redistribution (Dambly 2012; Horwell et al. 2013), except in special circumstances (e.g., in potassic magmas that also tend to be rich in fluorine; de Hoog et al. 2005).

In the White Island bomb, the recognition that SiO_2 in vapor-phase cristobalite was sourced from the corrosion rinds directly adjacent to isolated pores requires that the vapor responsible for silica redistribution had the capacity to break down aluminosilicate glass/melt, as well as the capacity to transport silica. HCl has limited capacity to directly uptake silica, as it tends to leach alkalis from adjacent glasses, but does not directly attack the silica framework (e.g., Schaeffer et al. 1986). Conversely, HF directly attacks the silicate framework of glasses to form SiF_4 (e.g., Zhang et al. 2012), and may therefore be crucial for vapor-phase cristobalite formation even if it is usually far less abundant than HCl in volcanic plumes.

Particularities of the magmatic system at White Island are useful in the discussion of halogen degassing, as previous work has indicated a clear demarcation of deep (> 500 m) and shallow degassing regimes separated by a zone of storage and phenocryst crystallization (Wardell et al. 2001; Kilgour et al. 2016). White Island is a major emitter of deeply derived CO_2 , H_2O , and SO_2 (Giggenbach 1975; Rose et al. 1986; Giggenbach 1987; Marty and Giggenbach 1990; Wardell et al. 2001; Werner et al. 2008), but melt inclusions in its pyroxene and plagioclase phenocrysts are low in all of these volatile species. Volatile solubility relationships indicate that these phenocrysts co-crystallize in shallow (100–500 m) storage, although phenocryst-melt equilibrium relationships suggest storage may be somewhat deeper (~ 1 km; Kilgour et al. 2016). Regardless, by the time magma reaches this main zone of storage and phenocryst crystallization, the majority of its original budget of CO_2 , H_2O , and S has already degassed (Wardell et al. 2001). Distinct deep- and shallow-degassing regimes associated with shallow magmatic plug crystallization, evolution, and eventual disruption are not unique to White Island, for example, having been documented at Stromboli by analysis of bomb textures, melt inclusions, and gas compositions (Polacci et al. 2006; Burton et al. 2007; Métrich et al. 2010; Gurioli et al. 2014). At shallow conduit

depths of plug formation at White Island, only residual H_2O , Cl, and/or F remain available for degassing, and it is therefore justified to treat these in isolation from deeper-derived volatile species.

As a first-order investigation of the relationship between halogen degassing and vapor-phase cristobalite formation at White Island, we apply a halogen degassing + crystallization model (Villemant and Boudon 1999). Starting volatile concentrations in degassing models are taken as the average of all melt inclusion analyses reported in the literature, and we note that averages must be used because of the incomplete way data has been presented. Wardell et al. (2001) reported volatile contents from inclusions in scoria from 1989, but their data are presented variably as averages or ranges, and exclude fluorine. Rapien et al. (2003) analyzed inclusions from 1977 to 1989, but they presented some data as ranges, and variably included either chlorine or fluorine, but never both. Esposito et al. (2014) reported high-precision individual analyses of all volatile species (H_2O , CO_2 , S, Cl, F) in a suite of melt inclusions from 1989, but did not report compositions. These limitations notwithstanding, we note that major element compositions of plagioclase- and pyroxene-hosted melt inclusions did not change over the period 1977–1989 (Wardell et al. 2001; Rapien et al. 2003; and also Severs et al. 2009), and that there is significant overlap in major elements between these inclusions and the groundmass compositions measured in this work (Fig. 5a). We therefore consider the literature melt inclusion averages to reasonably approximate the melt in shallow storage at White Island at the time the investigated bomb erupted (1999). Final volatile contents in our models are taken as the matrix H_2O estimated by FTIR and the average residual glass chlorine and fluorine measured by EPMA (Figs. 5b, c; Table 1).

Degassing of halogens is not fundamentally pressure-controlled (Métrich and Rutherford 1992), but is associated with partitioning into H_2O vapor exsolved at low pressures (Balcone-Boissard et al. 2010). Partitioning between vapor (v) and melt (m) is described by partition coefficients $D_X^{v/m} = [X]_v/[X]_m$, the final concentration in the melt ($[X]_m$) relative to initial concentration ($[X]_i$) of each halogen X . Halogens diffuse slowly compared to H_2O , so that partitioning into exsolved vapor is kinetically limited (Baker and Balcone-Boissard 2009). Furthermore, Cl and F are incompatible in most microlite phases, so that they become enriched in residual melt during groundmass crystallization. These factors promote halogen degassing from slowly cooled magma bodies in which groundmass crystallization is extensive and partitioning can proceed to equilibrium. The effects of this relationship have been observed even for chemically equivalent magmas with identical halogen budgets, as explosive eruptions involving rapid magma ascent and rapid quenching degas halogens less

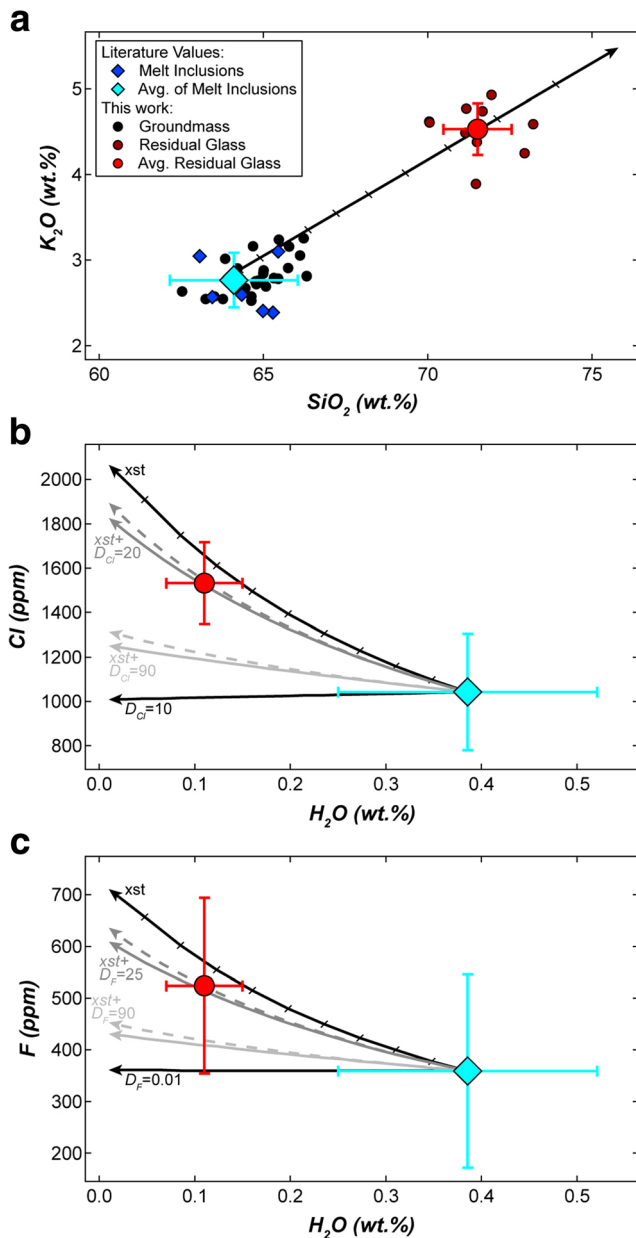


Fig. 5 Geochemistry and halogen degassing models. **a** K_2O versus SiO_2 . Melt inclusions are shown as individual points and average for the 1977–1989 eruptive period at White Island (Wardell et al. 2001; Rapien et al. 2003; Severs et al. 2009), and overlap with groundmass (defocused beam) compositions measured in this work. The ten most-evolved (e.g., least contaminated by microlites) residual glass (focused beam) compositions and their average are shown for the 1999 bomb studied here. The arrow represents evolution of melt composition due to crystallization of the observed microlite assemblage (plg + cpx) in 5% increments. **b, c** Halogen partitioning models during shallow H_2O degassing. Initial volatile concentrations are the average of melt inclusion analyses for 1977–1989 (Wardell et al. 2001; Rapien et al. 2003; Esposito et al. 2014), and final volatile concentrations are as measured in this work (Table 1). Models for chlorine (**b**) and fluorine (**c**) evolution in the melt are shown for cases of degassing (labeled with partition coefficients, D_X), crystallization (xst), and crystallization + degassing (xst + D_X) in closed (solid) and open (dashed) systems

prodigiously than effusive eruptions involving slow ascent and slow cooling (Villemant and Boudon 1999; Edmonds et al. 2002; Villemant et al. 2008; Lowenstern et al. 2012).

Equilibrium partition coefficients ($D_{Cl}^{v/m}$, $D_F^{v/m}$) are dependent on melt composition (especially alkalinity; Metrich and Rutherford 1992), pressure, and temperature, but there is a significant lack of experimental data for partitioning at the low pressures (< 50 MPa) of shallow conduits and/or effusive lava bodies (see Balcone-Boissard et al. 2010 and references therein). Typical $D_{Cl}^{v/m}$ are on the order of 10–50 for closed-system degassing (i.e., bubbles remain isolated from surroundings and one another) and significantly higher for open-system degassing, whereas $D_F^{v/m}$ is usually considered to be $\ll 1$ (Villemant and Boudon 1999; Harford et al. 2003; Villemant et al. 2008). The model of Villemant and Boudon (1999) modified by Harford et al. (2003) accommodates microlite crystallization (S) occurring with H_2O degassing by a factor $k = S/([H_2O]_i - [H_2O]_m)$, such that a bulk partition coefficient can be defined as

$$D_X^B = D_X^{v/m} / (1 + k) \tag{1}$$

and the fraction of melt remaining after each degassing and/or crystallization step is

$$f = 1 - (1 + k) ([H_2O]_i - [H_2O]_m) \tag{2}$$

These are combined to calculate the $[X]_m$, either in a closed system

$$[X]_m = [X]_i / [(1 - D_X^B)f + D_X^B] \tag{3}$$

or in an open system

$$[X]_m = [X]_i f^{D_X^{v/m} - 1} \tag{4}$$

during exsolution of H_2O with declining pressure. Figure 5b, c shows degassing with and without crystallization (xst) models for chlorine and fluorine for the cristobalite-bearing White Island bomb for a range of $D_{Cl}^{v/m}$ and $D_F^{v/m}$.

Both chlorine and fluorine in the White Island bomb are enriched in the residual glass compared to melt inclusions, consistent with halogen incompatibility during microlite crystallization (Fig. 5b, c). The final chlorine concentration, however, is less than that expected for pure crystallization, and is best predicted by a model that combines ~ 37% groundmass crystallization and closed-system partitioning with $D_{Cl}^{v/m}$ of ~ 20 (Fig. 5b). The final fluorine concentration is also less than expected for pure crystallization, and is best approximated by a crystallization + partitioning model using a rather high $D_F^{v/m}$ of ~ 25. Large variability in chlorine and fluorine in residual glass is reflected in the plus and minus one

standard deviation error bars of Fig. 5b, c. This is partly an analytical effect but also might be expected given that the slow diffusion of these elements may lead to high spatial heterogeneity in the residual glass (e.g., Lowenstern et al. 2012). Furthermore, assessment of the model is dependent on the final H₂O content, for which our FTIR measurements are only indicative. Given the large error bars on both starting and final compositions, the models should be viewed as semi-quantitative, but the salient point is that they indicate significant partitioning of both chlorine and fluorine into H₂O vapor generated by low-pressure degassing in a closed system (e.g., into isolated bubbles).

The best-fit chlorine degassing model ($x_{st} + D_{Cl}^{v/m} \sim 20$) predicts the HCl/H₂O molar ratio of fluid in the isolated vesicles to be 0.019 (calculated by $[Cl_m]_{xst} - [Cl_m]_{xst + D_{Cl}^{v/m} = 20}$), which is significantly higher than the multi-decadal HCl/H₂O average of ~ 0.004 in White Island gas emissions (e.g., Wardell et al. 2008 and references therein), but lower than the maximum measured HCl/H₂O of 0.023 (Giggenbach 1975). The best-fit fluorine degassing model ($x_{st} + D_F^{v/m} \sim 25$) predicts the HF/H₂O molar ratio to be 0.015, which appears to be very high, as HF is generally around 4 orders of magnitude less abundant than HCl in plume gases from White Island (Wardell et al. 2008). Given that we have modeled closed-system partitioning of halogens into isolated bubbles, chlorine and fluorine concentrations that are high relative to the bulk plume measurements are not surprising. It is likely that halogen species measured in the White Island plume (e.g., escaping in an open system rather than entrapped in isolated pores) are significantly diluted by deeply derived H₂O and other gases fluxing through the magmatic system from depth (Wardell et al. 2001). Furthermore, it has been noted that HF/HCl ratios in White Island plumes and fumaroles are highly variable, owing to the presence of an active hydrothermal system at White Island and the high solubility of HF in water (Wardell et al. 2008). The results of our analyses and modeling indicate two key items: (1) that even if a volcanic edifice outputs a bulk plume with relatively low HCl and HF, the isolated bubbles within the magma may contain significantly higher proportions of these species, which is capable of corroding the residual glass and depositing vapor-phase cristobalite; and more generally, (2) that pore space formed at different points in a given magma's evolution will contain vapor of different compositions.

Sequence of events leading to cristobalite formation

Textural features of the White Island bomb, informed by semi-quantitative halogen degassing models and previous work at White Island, permit a spatiotemporal sequence of degassing and textural evolution to be reconstructed (Fig. 6). The sequence of events is not different from previous models for

local SiO₂ distribution (Damby 2012; Horwell et al. 2013), but refined by the pristine textures presented here.

The connected vesicles represent a mature bubble population that has undergone nucleation, growth, and coalescence into a permeable network, whereas the isolated, cristobalite-bearing vesicles represent juvenile bubbles that have not coalesced. Having the connected pore network become established at depth could provide the permeability required to sustain long-term open-system flux of CO₂ + SO₂ + H₂O from White Island, but this can only be reconciled with melt inclusion studies if it were established deep in the magmatic system, below the shallow zone of phenocryst crystallization (Wardell et al. 2001).

The sub-spherical shape of the isolated vesicles, and the fact that they lack any short-lengthscale evidence for interaction with a rigid but permeable network of microlites (e.g., Schipper et al. 2012), indicates that they grew in a relatively continuous melt. The formation of groundmass microlites probably assisted in driving this vesiculation through second boiling, but at least some proportion of microlites must have formed after the secondary population of bubbles had been established; otherwise, the bubble shapes would have been dictated by the rigid microlite network. Equivalent microlite abundances in the bulk groundmass and in corrosion rinds indicate that corrosion occurred after groundmass crystallization was complete. Deposition of cristobalite crystals in the isolated pores requires that the vapor had become saturated in SiO₂, necessarily after corrosion had advanced.

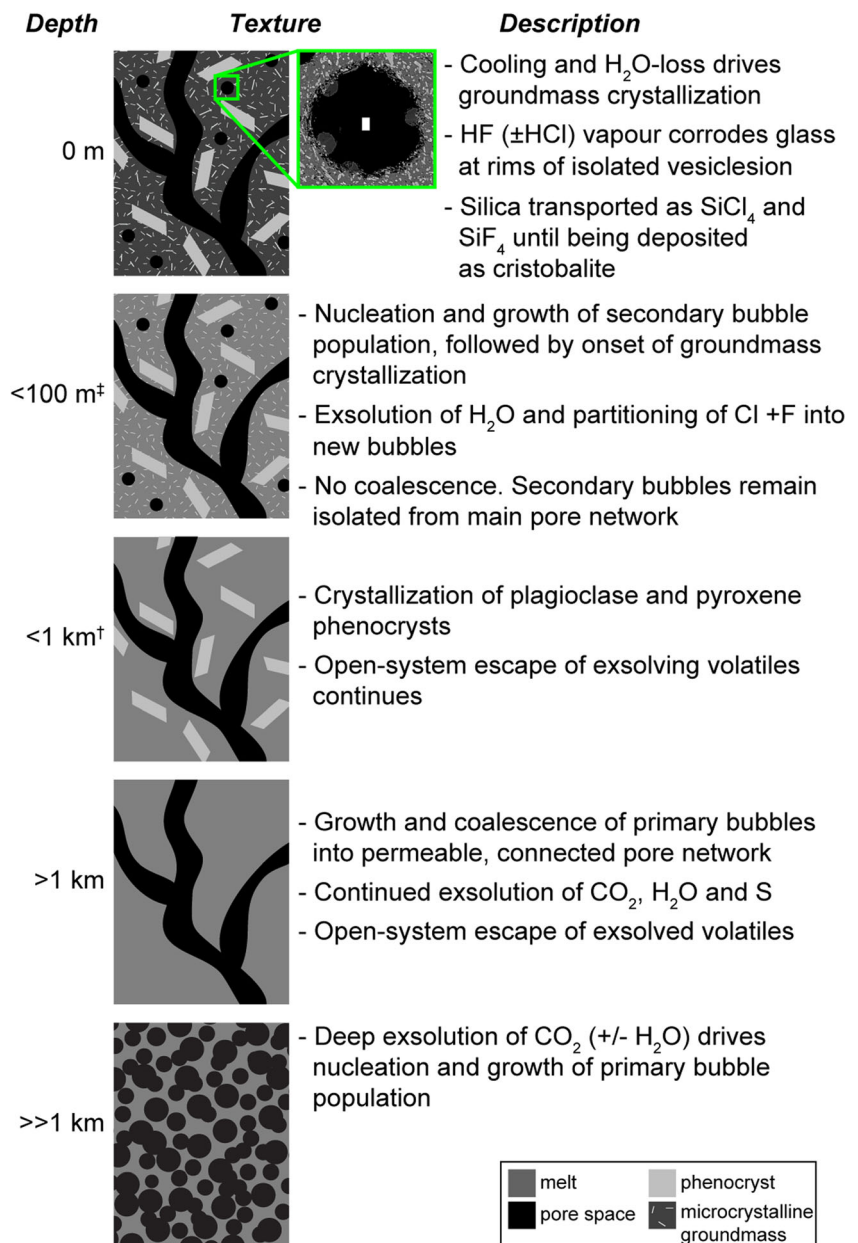
The overall sequence of events is therefore (1) deep bubble growth and evolution into a connected pore network from which CO₂ + SO₂ + H₂O could escape; (2) phenocryst growth in shallow storage; (3) secondary bubble nucleation and growth by exsolution of residual H₂O in the shallow conduit, concurrent with (4) groundmass crystallization and contemporaneous (5) partitioning of chlorine and fluorine into exsolved vapor; (6) corrosion of isolated bubble walls until vapor reached silica saturation; (7) deposition of cristobalite; and (8) explosive fragmentation of the volcanic plug material to eject and quench the White Island bomb.

Utility of cristobalite as an indicator of magmatic processes

The observations that vapor-phase cristobalite forms in response to halogen degassing, and that it forms preferentially in isolated vesicles, makes its presence a useful textural indicator of several conduit processes that are often difficult to distinguish in volcanic rocks.

Slow halogen diffusion dictates that the fluids required to redistribute SiO₂ are only produced in cases where magma has a protracted cooling and crystallization history (Balcone-Boissard et al. 2010). The links between halogen degassing

Fig. 6 Summary of textural evolution and volatile exsolution leading to deposition of vapor-phase cristobalite at White Island. Any phenocrysts or xenocrysts that formed or were carried from deeper than the indicated zone of plagioclase and pyroxene crystallization (some clasts from the same period of activity from White Island also contained rare olivine) are not represented in this schematic. †Phenocryst growth is restricted to < 1 km depth, as indicated by melt inclusion volatile contents (Wardell et al. 2001) and petrological models (Kilgour et al. 2016). ‡Growth of secondary bubble population at < 100 m is inferred from the residual H₂O contents (Table 1), and corroborated by literature values for matrix glass H₂O contents and solubility relationships for White Island dacite (Wardell et al. 2001; Rapien et al. 2003)



and slow magma cooling are well established, captured from analysis of eruption products (Villemant and Boudon 1999; Harford et al. 2003; Villemant et al. 2008; Lowenstern et al. 2012) and measurement of syn-eruptive gas emissions (Edmonds et al. 2002), but these approaches require detailed analytical work and/or syn-eruptive fieldwork. We suggest that the presence of vapor-phase cristobalite provides immediate evidence for halogen degassing under slow-cooling, equilibrium conditions, and is related to microlite crystallization and associated second boiling. It therefore can be used as a complement to textural quantification of vesicle and microlite populations, to infer which bubbles formed at low pressures, and the relative cooling histories of co-erupted materials.

Secondly, gas permeability plays a central role in volcanic explosivity, with closed-system degassing promoting rapid ascent and fragmentation, and open-system degassing promoting slow ascent and quiet effusion (Eichelberger et al. 1986). These processes are typically described as end members controlling the eruptive fate of a given magma. However, given that solubility of all major volatile species (e.g., CO₂, H₂O, S, Cl, F) are controlled by different variables (e.g., pressure, oxidation state, fluid partitioning), gases of different compositions exsolve from the melt under different conditions and at different times, and necessarily form and/or encounter vastly different pore structures in a magma body that is texturally maturing. The White Island bomb examined

here demonstrates that open-system (i.e., permeable) and closed-system (i.e., impermeable) degassing can occur simultaneously—the former allowing discharge of both deeply (CO₂, H₂O, S) and shallowly derived (residual H₂O, Cl, F) volatiles into a bulk plume, and the latter retaining vapors composed of only the shallowly derived species. The presence of vapor-phase cristobalite can thus indicate that shallow, closed-system chlorine and fluorine degassing was an integral part of a given magma ascent history.

Finally, the vesicles preserved in volcanic rocks are important textural indicators of degassing processes; however, being subject to resorption, compaction, deformation, and coalescence, primary vesicle textures are readily syn- and post-eruptively overprinted during conduit flow, in pyroclasts, and in lava domes and flows (Thomas and Sparks 1992; Cashman and Mangan 1994; Stovall et al. 2010; McIntosh et al. 2014; Kennedy et al. 2016). The association between vapor-phase cristobalite and isolated porosity documented here means that the presence of cristobalite in volcanic rocks can be used as a proxy for where isolated vesicles *had been* during late-stage degassing, even if the host vesicle itself subsequently collapsed, was deformed, or coalesced with adjacent pores. This is particularly applicable to the interpretation of lava domes and flows, if we consider upscaling of lava volumes—and therefore volatile budgets and cooling rates—from the small bomb studied here to large bodies of silicic lava. For example, in the 2011–2012 Cordón Caulle rhyolite flow (Chile), vapor-phase cristobalite was found in vesicles that were variably connected and isolated, and the presence of what appeared to be fragments of vapor-phase cristobalite crystals was present in lava flow core material that had been almost completely densified during emplacement (see Fig. 3 of Schipper et al. 2015). The new information presented here suggests that all vapor-phase cristobalite-bearing pore space was isolated during groundmass crystallization and cooling of the flow, before subsequent shearing caused partial coalescence, opening, and compaction of the pore network.

Cristobalite has traditionally been examined out of concern that it poses a respiratory health hazard to people living and working near persistently active volcanoes (Baxter et al. 1999). However, the low abundance and specific occurrence of cristobalite at White Island, at least in this particular example, can by no means be considered hazardous. Instead, we suggest that because vapor-phase cristobalite crystals are indicators of closed-system chlorine degassing accompanying groundmass crystallization, and because once formed they have higher preservation potential than the host vesicles in which they form, they are useful and durable complements to textural studies of volcanic rocks.

Conclusions

Cristobalite is not abundant in the investigated pyroclast from White Island, but its specific textural and geochemical characteristics illustrate details of the cristobalite forming process. (1) Cristobalite is present as a vapor-phase mineral, but not as a component of devitrified groundmass, indicating that these formation mechanisms occur independently. (2) Vapor-phase cristobalite is only present in isolated pores, despite the co-existence of a connected pore network. This indicates the effectiveness of local SiO₂ redistribution in impermeable portions of the magma. (3) Halogen degassing models show the most likely agent for glass corrosion and SiO₂ redistribution to be a mixture of concentrated HCl and HF, the production of halogen-rich fluids being promoted by slow cooling and the associated groundmass crystallization. Overall, we suggest that when vapor-phase cristobalite is observed in volcanic rocks, it indicates that the given rock had a protracted cooling history, during which it experienced significant halogen partitioning into H₂O-rich fluid phases, and that the distribution of vapor-phase cristobalite crystals mirrors the distribution of isolated pore space that existed in the magma during cooling. Although there remain significant uncertainties in the absolute rates of silica uptake and redistribution by corrosive vapor at magmatic temperatures that preclude the use of cristobalite as a quantitative speedometer, the relationships identified in this White Island bomb show that vapor-phase cristobalite can be used as durable, if qualitative, textural indicator of magmatic degassing and evolution processes that can be upscaled to explain more cryptic textures in larger lava bodies.

Acknowledgements Australian Synchrotron access was gained from proposal 2016/1-M10503 and supported by the New Zealand Synchrotron Group. CIS acknowledges a VUW faculty strategic research grant 212525/3620, A. Möbis for access to FTIR facilities at Massey University, and the staff of the Otago Centre for Electron Microscopy for their valuable support. We also thank T. Shea and H. Balcone-Boissard for constructive reviews that helped to improve this work.

References

- Baker DR, Balcone-Boissard H (2009) Halogen diffusion in magmatic systems: our current state of knowledge. *Chem Geol* 263:82–88. <https://doi.org/10.1016/j.chemgeo.2008.10.010>
- Baker DR, Mancini L, Polacci M, Higgins MD, Gualda GAR, Hill RJ, Rivers ML (2012) An introduction to the application of X-ray microtomography to the three-dimensional study of igneous rocks. *Lithos* 148:262–276. <https://doi.org/10.1016/j.lithos.2012.06.008>
- Balcone-Boissard H, Villement B, Boudon G (2010) Behaviour of halogens during the degassing of felsic magmas. *Geochem Geophys Geosys* 11:Q09005. <https://doi.org/10.1029/2010GC003028>
- Baxter PJ, Bonadonna C, Dupree R, Hards VL, Kohn SC, Murphy MD, Nichols A, Nicholson RA, Norton GE, Searl A, Sparks RSJ, Vickers BP (1999) Cristobalite in volcanic ash of the Soufriere Hills Volcano, Montserrat, British West Indies. *Science* 283:1142–1145

- Best MG (2003) *Igneous and metamorphic petrology*, Second edn. Blackwell Publishing, Malden, p 729
- Boudon G, Balcone-Boissard H, Villemant B, Morgan DJ (2015) What factors control superficial lava dome explosivity? *Sci Reps* 5:14551. <https://doi.org/10.1038/srep14551>
- Burton M, Allard P, Mure F, La Spina A (2007) Magmatic gas composition reveals the source depth of slug-driven strombolian explosive activity. *Science* 317:227–230
- Cashman KV, Mangan MT (1994) Physical aspects of magmatic degassing: II, constraints on vesiculation processes from textural studies of eruptive products. In: Carroll MR, Holloway JR (eds) *Volatiles in magmas, reviews in mineralogy*. pp 447–478
- Churakov SV, Tkachenko SI, Korzhinskii MA, Bocharnikov RE, Schmulovich KI (2000) Evolution of composition of high-temperature fumarolic gases from Kudryavy Volcano, Iturup, Kuril Islands: the thermodynamic modeling. *Geochem Int* 38:436–451
- Cole JW, Thordarson T, Burt RM (2000) Magma origin and evolution of White Island (Whakaari) volcano, Bay of Plenty, New Zealand. *J Petrol* 41:867–895
- Damby DE (2012) From dome to disease: the respiratory toxicity of volcanic cristobalite. In: Department of Earth Sciences. Durham University, Durham, p 359
- Damby DE, Llewellyn EW, Horwell CJ, Williamson BJ, Najorka J, Cressey G, Carpenter M (2014) The α - β phase transition in volcanic cristobalite. *J Appl Crystallogr* 47:1205–1215. <https://doi.org/10.1107/S160057671401070X>
- de Hoog JCM, van Bergen MJ, Jacobs MHG (2005) Vapour-phase crystallisation of silica from SiF₄-bearing volcanic gases. *Ann Geophys* 48:775–785
- Deer WA, Howie RA, Zussman J (1992) *An introduction to the rock-forming minerals*, 2nd edn. John Wiley and Sons, New York
- Duncan AR (1970) The petrology and petrochemistry of andesite and dacite volcanoes in Eastern Bay of Plenty, New Zealand. In: *Geology*. Victoria University of Wellington, Wellington, p 360
- Edmonds M, Pyle DM, Oppenheimer C (2002) HCl emissions at Soufrière Hills Volcano, Montserrat, West Indies, during a second phase of dome building: November 1999 to October 2000. *Bull Volcanol* 64:21–30. <https://doi.org/10.1007/s00445-001-0175-0>
- Edmonds M, Wallace PJ (2017) Volatiles and exsolved vapor in volcanic systems. *Elements* 13:29–34. <https://doi.org/10.2113/gselements.13.1.29>
- Eichelberger JC, Carrigan CR, Westrich HR, Price RH (1986) Non-explosive silicic volcanism. *Nature* 323:598–602. <https://doi.org/10.1038/323598a0>
- Esposito R, Hunter J, Schiffbauer JD, Shimizu N, Bodnar RJ (2014) An assessment of the reliability of melt inclusions as recorders of the pre-eruptive volatile content of magmas. *Am Mineral* 99:976–998. <https://doi.org/10.2138/am.2014.4574>
- GeoNet (2017) White Island Alert Level <https://www.geonet.org.nz/volcano/whiteisland>, accessed Sept 13, 2017
- Giggenbach WF (1975) Variations in the carbon, sulfur and chlorine contents of volcanic gas discharges from White Island, New Zealand. *Bull Volcanologique* 39:15–27
- Giggenbach WF (1987) Redox processes governing the chemistry of fumarolic gas discharges from White Island, New Zealand. *Appl Geochem* 2:143–161
- Gillet P, Le Cléac'h A (1990) High-temperature raman spectroscopy of SiO₂ and GeO₂ polymorphs: anharmonicity and thermodynamic properties at high-temperatures. *J Geophys Res* 95(B13):21635–21655. <https://doi.org/10.1029/JB095iB13p21635>
- Global Volcanism. Program (1998) Report on White Island (New Zealand). In: Wunderman R (ed) *Bulletin of the Global Volcanism Network*. Smithsonian Institution, p 8
- Global Volcanism. Program (2013) WHITE ISLAND (241040). In: Venzke E (ed) *Volcanoes of the world*. Smithsonian Institution. <https://www.geonet.org.nz/volcano/whiteisland>, accessed Sept 13, 2017. doi:<https://doi.org/10.5479/si.GVP.VOTW4-2013>
- Gurioli L, Colo L, Bollasina AJ, Harris AJL, Whittington A, Ripepe M (2014) Dynamics of Strombolian explosions: inferences from field and laboratory studies of erupted bombs from Stromboli volcano. *J Geophys Res Solid Earth* 119:319–345. <https://doi.org/10.1002/2013JB010355>
- Harford CL, Sparks RSJ, Fallick AE (2003) Degassing at the Soufrière Hills volcano, Montserrat, recorded in matrix glass compositions. *J Petrol* 44:1503–1523
- Heaney PJ (1994) Structure and chemistry of the low-pressure silica polymorphs. *Rev Mineral* 29:1–40
- Horwell CJ, Baxter PJ (2006) The respiratory health hazards of volcanic ash: a review for volcanic risk mitigation. *Bull Volcanol* 69:1–24. <https://doi.org/10.1007/s00445-006-0052-y>
- Horwell CJ, Hillman SE, Cole PD, Loughlin SC, Llewellyn EW, Damby DE, Christopher TE (2014) Controls on variations in cristobalite abundance in ash generated by the Soufrière Hills Volcano, Montserrat in the period 1997–2010. *Geol Soc London Memoirs* 39:399–406. <https://doi.org/10.1144/M39.21>
- Horwell CJ, Le Blond JS, Michnowicz SAK, Cressey G (2010) Cristobalite in a rhyolitic lava dome: evolution of ash hazard. *Bull Volcanol* 72:249–253. <https://doi.org/10.1007/s00445-009-0327-1>
- Horwell CJ, Williamson BJ, Llewellyn EW, Damby DE, Le Blond JS (2013) The nature and formation of cristobalite at the Soufrière Hills volcano, Montserrat: implications for the petrology and stability of silicic lava domes. *Bull Volcanol* 75:696. <https://doi.org/10.1007/s00445-013-0696-3>
- Houghton BF, Nairn IA (1991) The 1976–1982 Strombolian and phreatomagmatic eruptions of White Island, New Zealand: eruptive and depositional mechanisms at a 'wet' volcano. *Bull Volcanol* 54: 25–49
- Jarosewich E, Nelen JA, Norberg JA (1980) Reference samples for electron microprobe analysis. *Geostand Newslett* 4:43–47
- Kennedy BM, Wadsworth FB, Vasseur J, Schipper CI, Jellinek AM, von Aulock FW, Hess K-U, Russell JK, Lavallée Y, Nichols ARL, Dingwell DB (2016) Surface tension driven processes densify and retain permeability in magma and lava. *Earth Planet Sci Lett* 433: 116–124. <https://doi.org/10.1016/j.epsl.2015.10.031>
- Kilgour G, Moune S, Della Pasqua F, Christenson BW (2016) Petrological insights into the 1976–2000 eruption episode of White Island, New Zealand: an eruption fuelled by repeated mafic recharge. *Geophysical Research Abstracts*, EGU General Assembly, Vienna, 18
- Kingma KJ, Hemley RJ (1994) Raman spectroscopic study of microcrystalline silica. *Am Mineral* 79:269–273
- Le Maitre RW, Bateman P, Dudek A, Keller J, Lameyre J, Le Bas MJ, Sabine PA, Schmid R, Sorensen H, Streckeisen A, Wooley AR, Zanettin B (1989) *A classification of igneous rocks and glossary of terms: recommendations of the International Union of Geological Sciences Subcommittee on the Systematics of Igneous Rocks*. Blackwell Scientific Publications, Oxford
- Limaye A (2012) *Drishti: a volume exploration and presentation tool*. Developments in X-Ray Tomography VIII 85060X
- Lowenstern JB, Bleick H, Vazquez JA, Castro JM, Larson PB (2012) Degassing of Cl, F, Li, and Be during extrusion and crystallization of the rhyolite dome at Volcán Chaitén, Chile during 2008 and 2009. *Bull Volcanol* 74:2303–2319. <https://doi.org/10.1007/s00445-012-0663-4>
- Marty B, Giggenbach WF (1990) Major and rare gases at White Island volcano, New Zealand: origin and flux of volatiles. *Geophys Res Lett* 17:247–250. <https://doi.org/10.1029/GL017i003p00247>
- McIntosh IM, Llewellyn EW, Humphreys MCS, Nichols ARL, Burgisser A, Schipper CI, Larsen JF (2014) Distribution of dissolved water in magmatic glass records growth and resorption of bubbles. *Earth Planet Sci Lett* 401:1–11. <https://doi.org/10.1016/j.epsl.2014.05.037>

- Métrich N, Bertagnini A, Di Muro A (2010) Conditions of magma storage, degassing and ascent at Stromboli: new insights into the volcano plumbing system with inferences on the eruptive dynamics. *J Petrol* 51:603–626. <https://doi.org/10.1093/petrology/egp083>
- Métrich N, Rutherford MJ (1992) Experimental study of chlorine behavior in hydrous silicic melts. *Geochim Cosmochim Acta* 56:607–616
- Murtagh RM, White JDL (2013) Pyroclast characteristics of a subaqueous to emergent Surtseyan eruption, Black Point volcano, California. *J Volcanol Geotherm Res* 267:75–91. <https://doi.org/10.1016/j.jvolgeores.2013.08.015>
- Okumura S, Nakamura M, Nakashima S (2003) Determination of molar absorptivity of IR fundamental OH-stretching vibration in rhyolitic glasses. *Am Mineral* 88:1657–1662
- Polacci M, Corsaro RA, Andronico D (2006) Coupled textural and compositional characterization of basaltic scoria; insights into the transition from Strombolian to fire fountain activity at Mount Etna, Italy. *Geology* 34:201–204
- Rapien MH, Bodnar RJ, Simmons SF, Szabo CS, Wood CP, Sutton SR (2003) Melt inclusion study of the embryonic porphyry copper system at White Island, New Zealand. *Soc Econ Geol Spec Pub* 10:41–59
- Rose WI, Chuan RL, Giggenbach WF, Kyle PR, Symonds RB (1986) Rates of sulfur dioxide and particle emissions from White Island volcano, New Zealand, and an estimate of the total flux of major gas species. *Bull Volcanol* 48:181–188
- Rust AC, Manga M, Cashman KV (2003) Determining flow type, shear rate and shear stress in magmas from bubble shapes and orientations. *J Volcanol Geotherm Res* 122:111–132
- Sable JE, Houghton BF, Wilson CJN, Carey RJ (2009) Eruption mechanisms during the climax of the Tarawera 1886 basaltic Plinian eruption inferred from microtextural characteristics of the deposits. In: Thordarson T, Self S, Larsen G, Rowland SK, Hoskuldsson A (eds) *Studies in volcanology: the legacy of George Walker*. Geological Society, London, pp 129–154
- Schaeffer HA, Stengel M, Mecha J (1986) Dealkinization of glass surfaces utilizing HCl gas. *J Non-Cryst Solid* 80:400–404
- Schipper CI, Castro JM, Tuffen H, Wadsworth FB, Chappell D, Pantoja AE, Simpson M, Le Ru EC (2015) Cristobalite in the 2011–12 Cordón Caulle eruption (Chile). *Bull Volcanol* 77:34. <https://doi.org/10.1007/s00445-015-0925-z>
- Schipper CI, White JDL, Nichols ARL, Burgisser A, Hellebrand E, Murtagh R (2012) Incipient melt segregation as preserved in subaqueous pyroclasts. *Geology* 40:355–358. <https://doi.org/10.1130/G32582.1>
- Schneider CA, Rasband WS, Eliceiri KW (2012) NIH Image to ImageJ: 25 years of image analysis. *Nat Methods* 9:671–675
- Severs MJ, Beard JS, Fedele L, Hanchar JM, Mutchler SR, Bodnar RJ (2009) Partitioning behavior of trace elements between dacitic melt and plagioclase, orthopyroxene, and clinopyroxene based on laser ablation ICPMS analysis of silicate melt inclusions. *Geochim Cosmochim Acta* 73:2123–2141. <https://doi.org/10.1016/j.gca.2009.01.009>
- Shea T, Houghton BF, Gurioli L, Cashman KV, Hammer JE, Hobden BJ (2010) Textural studies of vesicles in volcanic rocks: an integrated methodology. *J Volcanol Geotherm Res* 190:271–289. <https://doi.org/10.1016/j.jvolgeores.2009.12.003>
- Shmulovich KI, Yardley BWD, Graham CM (2006) Solubility of quartz in crustal fluids: experiments and general equations for salt solutions and H₂O-CO₂ mixtures at 400–800 °C and 0.1–0.9 GPa. *Geofluids* 6:154–167. <https://doi.org/10.1111/j.1468-8123.2006.00140.x>
- Stovall WK, Houghton BF, Gonnermann HM, Fagents SA, Swanson DA (2010) Eruption dynamics of Hawaiian-style fountains: the case study of episode 1 of the Kilauea Iki 1959 eruption. *Bull Volcanol* 73:511–529. <https://doi.org/10.1007/s00445-010-0426-z>
- Swanson SE, Naney MT, Westrich HR, Eichelberger JC (1989) Crystallization history of Obsidian Dome, Inyo Domes, California. *Bull Volcanol* 51:161–176
- Thomas RME, Sparks RSJ (1992) Cooling of tephra during fallout from eruption columns. *Bull Volcanol* 54:542–553. <https://doi.org/10.1007/BF00569939>
- Villemant B, Boudon G (1999) H₂O and halogen (F, Cl, Br) behaviour during shallow magma degassing processes. *Earth Planet Sci Lett* 168:271–286
- Villemant B, Mouatt J, Michel A (2008) Andesitic magma degassing investigated through H₂O vapour-melt partitioning of halogens at Soufrière Hills Volcano, Montserrat (Lesser Antilles). *Earth Planet Sci Lett* 269:212–229. <https://doi.org/10.1016/j.epsl.2008.02.014>
- von Aulock FW, Kennedy BM, Schipper CI, Castro JM, Martin DE, Oze C, Watkins JM, Wallace PJ, Puskar L, Bégué F, Nichols ARL, Tuffen H (2014) Advances in Fourier transform infrared spectroscopy of natural glasses: from sample preparation to data analysis. *Lithos* 206–207:52–64. <https://doi.org/10.1016/j.lithos.2014.07.017>
- Wardell LJ, Kyle PR, Counce D (2008) Volcanic emissions of metals and halogens from White Island (New Zealand) and Erebus volcano (Antarctica) determined with chemical traps. *J Volcanol Geotherm Res* 177:734–742. <https://doi.org/10.1016/j.jvolgeores.2007.07.007>
- Wardell LJ, Kyle PR, Dunbar N, Christenson B (2001) White Island Volcano, New Zealand: carbon dioxide and sulfur dioxide emission rates and melt inclusion studies. *Chem Geol* 177:187–200. [https://doi.org/10.1016/S0009-2541\(00\)00391-0](https://doi.org/10.1016/S0009-2541(00)00391-0)
- Werner C, Hurst T, Scott BJ, Sherburn S, Christenson BW, Britten K, Cole-Baker J, Mullan B (2008) Variability of passive gas emissions, seismicity, and deformation during crater lake growth at White Island Volcano, New Zealand, 2002–2006. *J Geophys Res* 113: B01204. <https://doi.org/10.1029/2007JB005094>
- Zhang YB, Xiao CF, An SL, Liu MT (2012) Hydrofluoric acid corrosion behaviour of SiO₂ glass used to prepare glass hollow fibre membrane. *Corr Eng Sci Tech* 47:456–462. <https://doi.org/10.1179/1478422X12Z.00000000057>